NANO LETTERS

pubs.acs.org/NanoLett

# A Comparison Study of the Catalytic Properties of Au-Based Nanocages, Nanoboxes, and Nanoparticles

Jie Zeng,[†] Qiang Zhang,[†] Jingyi Chen,[†] and Younan Xia*[,†,‡]

[†]Department of Biomedical Engineering, Washington University, St. Louis, Missouri 63130, and [‡]Department of Materials Science and Engineering, Yonsei University, Seoul, Korea

**ABSTRACT** We have evaluated the catalytic properties of Au-based nanostructures (including nanocages, nanoboxes, and solid nanoparticles) using a model reaction based on the reduction of *p*-nitrophenol by $NaBH_4$. From the average reaction rate constants at three different temperatures, we determined the activation energy, the entropy of activation, and the pre-exponential factor for each type of Au nanostructure. The kinetic data indicate that the Au-based nanocages are catalytically more active than both the nanoboxes and nanoparticles probably due to their extremely thin but electrically continuous walls, the high content of Au, and the accessibility of both inner and outer surfaces through the pores in the walls. In addition, a compensation effect was observed in this Au-based catalytic system, which can be primarily interpreted by a model based on kinetic regime switching.

**KEYWORDS** Gold, nanostructures, catalysts, *p*-nitrophenol, compensation effect

In the last decade or so, significant progress has been made with regard to the design, synthesis, and utilization of nanostructured materials.[1−6] Among various systems, noble-metal nanostructures have received great interest primarily due to their unique properties and applications in catalysis, photonics, electronics, and information storage.[4−8] Significantly, one can tailor the properties of noble-metal nanostructures and thus improve their performance in a variety of applications by controlling their size, shape, composition, and porosity (e.g., hollow vs solid). To this end, our group has developed a remarkably simple and versatile method based on the galvanic replacement reaction for generating noble-metal nanostructures with hollow interiors and/or porous walls, or more specifically in the form of nanocages or nanoboxes.[9−11] Subsequent studies have also demonstrated their great potential in a range of biomedical applications, including their use as contrast enhancement agents for modalities such as optical coherence tomography (OCT) and photoacoustic tomography (PAT), and as nanoscale transducers for photothermal treatment.[11−18]

The primary goal of this work is to quantitatively evaluate the catalytic properties of both Au-based nanocages and nanoboxes in comparison with Au solid nanoparticles. It is well-known that the catalytic activity of a nanoparticle is strongly dependent on its size. Typically, a smaller nanoparticle tends to show a higher catalytic activity as it has a much greater surface-to-volume ratio. This size dependence has been validated in a number of systems.[19,20] However, smaller nanoparticles may not be better candidates for catalyzing all types of reactions. A good example for explaining this exception can be found in a redox reaction. As the catalytic particles become increasingly smaller, the oxidation and reduction half reactions might need to occur on different particles due to the reduction in surface area. In this case, a good "electrical" connection between the particles will play an important role as the electrons have to be transported from the site of oxidation to the site of reduction. The redox reaction will be unable to proceed if the catalytic particles are separated from each other by an insulating medium. We argue that this kind of problem can be solved by switching from solid nanoparticles to nanocages or nanoboxes with hollow interiors and ultrathin walls. For a Au-based nanocage of 50 nm in edge length and 5 nm in wall thickness, it should be able to provide a sufficiently large surface area (at least, equivalent to a 50 nm solid particle) to accommodate both the oxidation and reduction half reactions while the ultrathin wall is still able to provide a high activity equivalent to a 5 nm solid particle due to a good electrical connection across the entire surface of the wall. For a model reaction based on the reduction of *p*-nitrophenol by sodium borohydride ($NaBH_4$), our experimental data indicate that both wall thickness and porosity of the Au-based hollow nanostructures play an important role in enhancing the catalytic activity.

By titrating Ag nanocubes with chloroauric acid ($HAuCl_4$) in an aqueous solution under refluxing, we were able to prepare three different types of Au-based hollow nanostructures—nanocages, nanoboxes, and partially hollow nanoboxes—through the galvanic replacement reaction (see the experimental details in Supporting Information).[10,21] Figure 1, parts A−C, shows transmision electron microscopy (TEM) images of these three types of nanostructures; the edge

* To whom correspondence should be addressed, xia@biomed.wustl.edu.
**Received for review:** 07/29/2009
**Published on Web:** 11/23/2009



DOI: 10.1021/nl903062e | *Nano Lett.* **2010,** *10,* 30-35

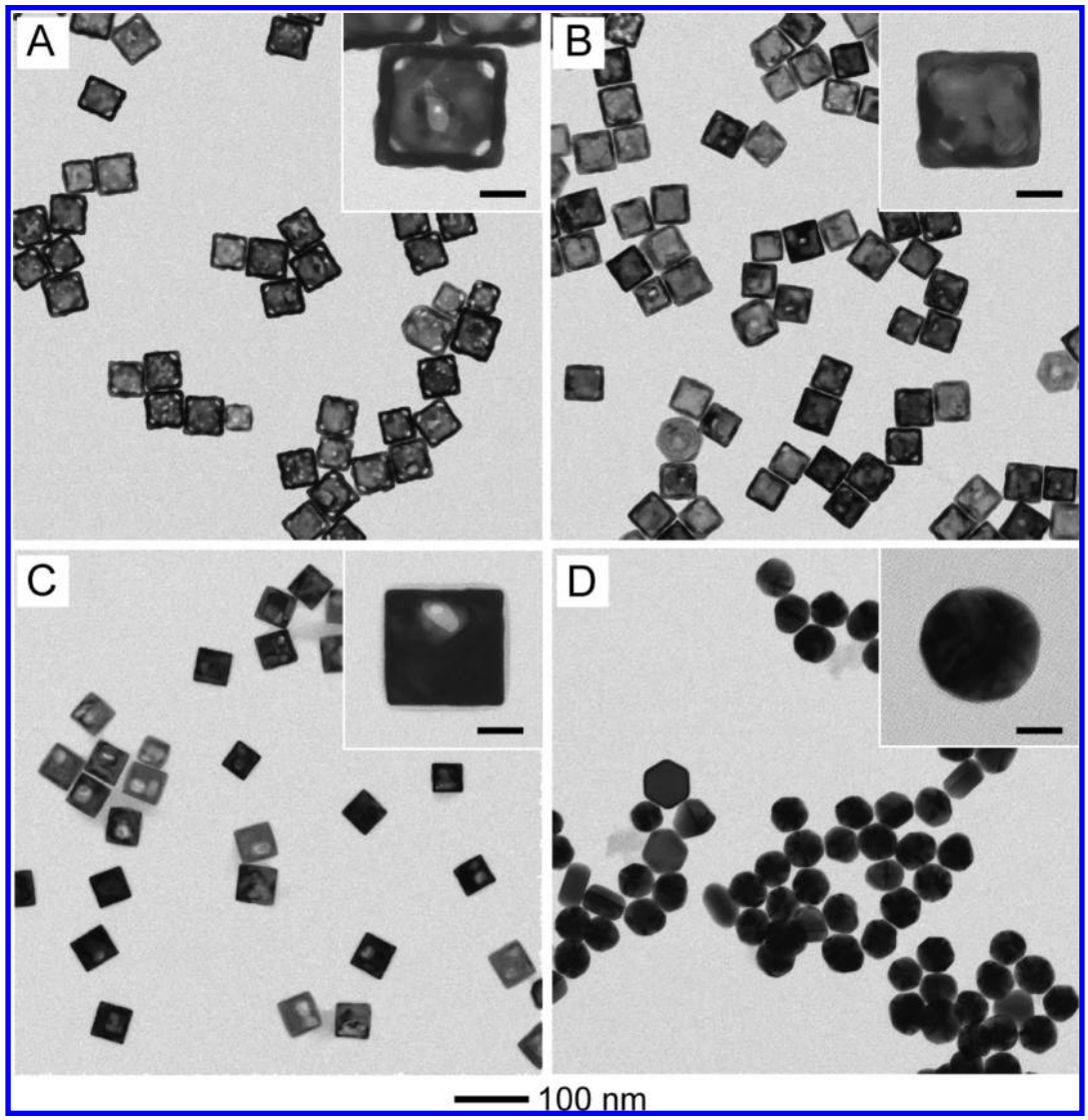


**FIGURE 1. TEM images of Au-based nanocages (A), nanoboxes (B), partially hollow nanoboxes (C), and solid nanoparticles (D) with an average size of 50 nm. The average wall thickness was 5 ± 2 nm for nanocages, 6 ± 3 nm for nanoboxes, and 13 ± 8 nm for partially hollow nanoboxes. The scale bars in the insets correspond to 20 nm.**

lengths were all around 50 nm since we used the same batch of Ag nanocubes for these syntheses. However, their porosity was quite different. The nanocages in Figure 1A exhibited the most porous morphology (with a complete hollow interior and essentially a pore at each corner) and the thinnest wall among these three types of hollow nanostructures. As for the nanoboxes (Figure 1B), their interiors were completely hollow and most of them showed slightly truncated corners. In the case of partially hollow nanoboxes (Figure 1C), there was still a significant amount of unreacted silver remaining inside each nanostructure although most of them showed one hole on the side face. Figure 1D and Figure S1 (in Supporting Information) show TEM images of two commercial samples of Au solid nanoparticles (Product 15708-5 and 15702-1, Ted Pella) with average diameters of 50 and 5 nm, respectively. These Au solid nanoparticles served as two references for benchmarking the catalytic activity of Au-based nanocages and nanoboxes.

We used the reduction of *p*-nitrophenol by $NaBH_4$ as a model system to quantitatively evaluate the catalytic activity of the gold nanostructures. The procedures were also described in detail in the Supporting Information. It is well-documented that this reaction can be catalyzed by noble-metal nanoparticles, and the color changes involved in the reduction also provide a simple way based on spectroscopic measurements for monitoring the reaction kinetics.[22,23] Under a neutral or acidic condition, *p*-nitrophenol solution exhibits a strong absorption peak at 317 nm. Upon the addition of $NaBH_4$, the alkalinity of the solution increased and *p*-nitrophenolate ions would become the dominating species, together with a spectral shift to 400 nm for the absorption peak.[24,25] After the Au-based catalyst was added



DOI: 10.1021/nl903062e | *Nano Lett.* **2010,** *10,* 30-35

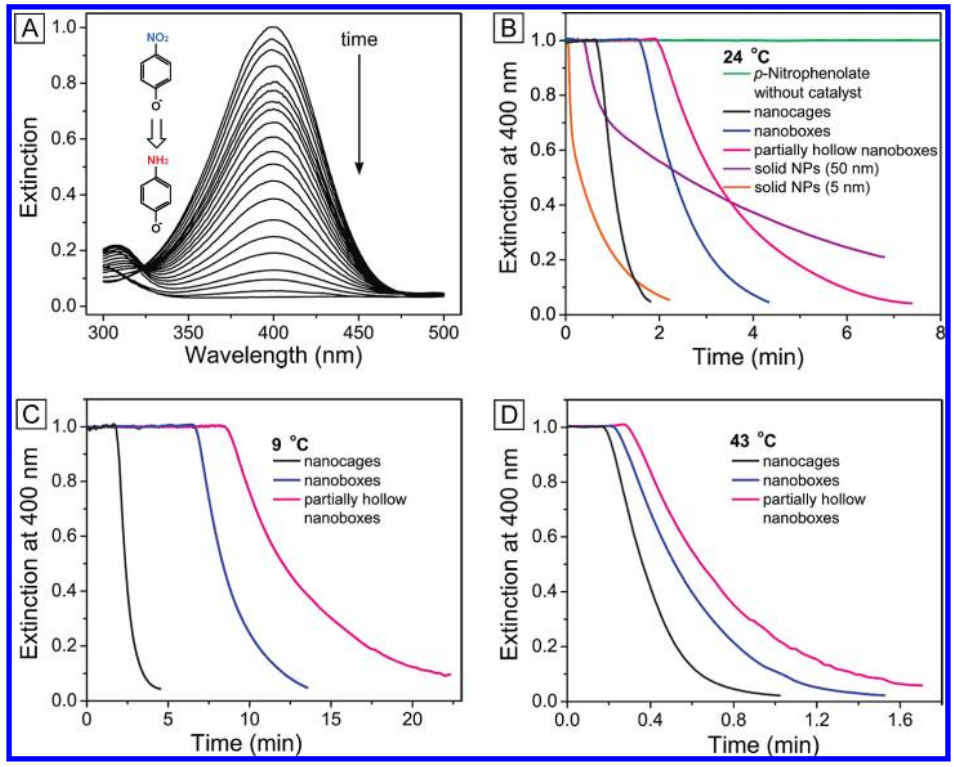


**FIGURE 2. (A) The extinction spectra at different reaction times, indicating the disappearance of the peak for *p*-nitrophenol due to the reduction of $-NO_2$ group into $-NH_2$ group. (B–D) Extinction (normalized against the initial point) at the peak position for *p*-nitrophenol (400 nm) as a function of time at three different temperatures: (B) 24 °C, (C) 9 °C, and (D) 43 °C. In all cases, the concentrations of *p*-nitrophenol and $NaBH_4$ were $1.4 \times 10^{-4}$ and $4.2 \times 10^{-2}$ M, respectively. The concentrations of Au-based catalyst are $3.8 \times 10^9$ particles/mL for nanocages, nanoboxes, partially hollow nanoboxes and 50 nm Au solid nanoparticles, and $1.56 \times 10^{12}$ particles/mL for 5 nm Au solid nanoparticles.**

(i.e., an aqueous dispersion of the nanocages, nanoboxes, or solid nanoparticles), the absorption peak at 400 nm gradually dropped in intensity as the reduction reaction proceeded (Figure 2A). At the same time, with the production of *p*-aminophenol, a new absorption peak started to rise as a shoulder at 315 nm.[24,25] Because the peak at 400 nm was much stronger than that at 315 nm, we decided to measure the concentrations of *p*-nitrophenolate ions and thus to monitor the progress or kinetics of the reaction by recording the absorbance at 400 nm. For all experiments, the initial concentrations of *p*-nitrophenol and $NaBH_4$ were kept at $1.4 \times 10^{-4}$ and $4.2 \times 10^{-2}$ M, respectively. The concentrations of Au-based catalyst were $3.8 \times 10^9$ particles/mL for nanocages, nanoboxes, partially hollow nanoboxes, and 50 nm Au solid nanoparticles, and $1.56 \times 10^{12}$ particles/mL for 5 nm small Au solid nanoparticles to keep the number of Au atoms roughly on the same scale for all other catalysts. Considering the nanocages and nanoboxes were all derived from the same batch of Ag nanocubes, we think it is reasonable to choose the particle concentration (the same as that of Ag nanocubes) as a base for comparison in terms of cost. For accuracy, the extinction caused by the Au-based catalyst was subtracted from all the spectroscopic measurements.

Figure 2B shows the experimental results obtained from the reaction conducted at room temperature (24 °C). Without the addition of Au-based catalyst, no reaction was observed. This observation indicates that the reduction reaction was unable to occur by itself under the experimental conditions. Upon the addition of a Au-based catalyst, regardless of the morphology, a certain period of time was required for the *p*-nitrophenol to adsorb onto the catalyst's surface before the reaction could be initiated. Here we define this period of time as the time of adsorption or $t_{ads}$. Among the different systems, the reaction catalyzed by Au nanocages showed the fastest rate and the shortest $t_{ads}$ as compared to both types of nanoboxes. A similar trend was also observed at a lower or higher temperature, for example, 9 and 43 °C, respectively (see Figure 2, C and D).

In our reaction system, the concentration of $BH_4^-$ greatly exceeded that of *p*-nitrophenol, so it is not unreasonable to consider its concentration as a constant during the reaction. The pseudo-first-order kinetics with respect to *p*-nitrophenol (or more accurately, *p*-nitrophenolate) could be applied to our experimental system.[24] The approximately linear shape of the plot of $-\ln I_{ext}$ ($I_{ext}$ represents the extinction intensity at 400 nm) versus time (after subtraction of $t_{ads}$), as shown in Figure 3, supports the pseudo-first-order assumption. According to the linear relationship, we calculated the average reaction rate constant ($k$) from three independent measurements for



DOI: 10.1021/nl903062e | *Nano Lett.* **2010,** *10,* 30-35

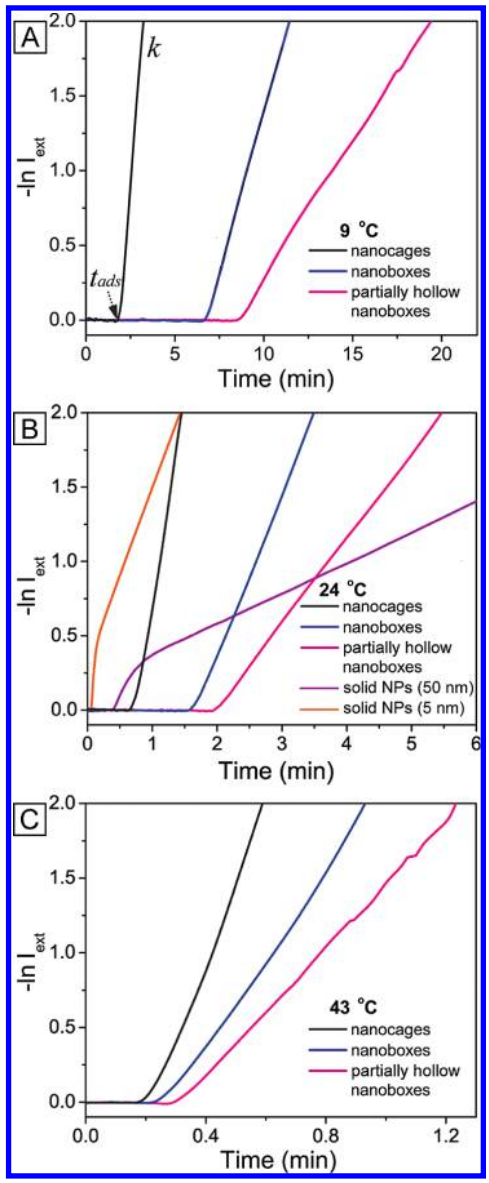


**FIGURE 3. Plots of $-\ln I_{ext}$ against time for Au-based nanocages, nanoboxes, and partially hollow nanoboxes at three different temperatures. For the plots at 24 °C, measurements for the Au solid nanoparticles of 50 and 5 nm in size are also included. These plots were then used to determine the reaction rate constant ($k$) and adsorption time ($t_{ads}$).**

each catalyst at three different temperatures, and summarized these data in Table 1. In addition, based on the linear fitting of ln $k$ versus 1000/$T$ and the Arrhenius equation

$$\ln k = \ln A - E_a/RT$$

we obtained the apparent activation energy ($E_a$) from the slope ($-E_a/R$). As seen in Figure 4A, the activation energy of nanoboxes (44.25 ± 2.62 kJ/mol) was lower than that of partially hollow nanoboxes (55.44 ± 3.15 kJ/mol), indicating a higher catalytic activity for the nanoboxes as their interiors became more empty. We have demonstrated that the partially hollow nanoboxes consisted of a Au−Ag alloyed surface in the initial stage of galvanic replacement (Figure 1C) while a dealloying process would be initiated when the corners of the nanoboxes became slightly truncated (Figure 1B).[21] Consequently, the result of a lower value of $E_a$ for completely hollow nanoboxes relative to partially hollow nanoboxes can be attributed to the much thinner walls associated with a completely empty nanobox and the increased Au/Ag ratio due to dealloying of Ag from the surface. Since the Ag atoms located on the surface of a Au−Ag alloyed nanobox could not catalyze the reaction, their presence is expected to hinder the catalytic process. It is worth noting that the activation energy of the nanocages (28.04 ± 1.43 kJ/mol) was significantly lower than both samples of nanoboxes. This substantial increase in catalytic activity can be explained from three different angles: (i) the nanocages had the thinnest walls among the three types of hollow nanostructures; (ii) the dealloying process made the Au/Ag ratio (or the number of effective catalytic sites) on the surface of a nanocage much higher than those of both types of nanoboxes;[21] and (iii) the multiple holes at the corners of the nanocage allow both the outer and inner surfaces to serve as catalytic sites.

In addition to activation energy, the pre-exponential factor ($A$) can be calculated from the intercept of the linear dependence of ln $k$ versus 1000/$T$, and the entropy of activation ($\Delta S$) can be obtained from the equation $\ln A = \Delta S/R$.[26] These data are summarized in Table 2. It is clear that the reaction involving nanocages had the lowest pre-exponential factor and entropy of activation, while the reaction involving partially hollow nanoboxes had the highest pre-exponential factor and entropy of activation. The nanoboxes gave pre-exponential factor and entropy of activation that were situated between those values observed for nanocages and partially hollow nanoboxes.

The linear relationship of ln $A$ versus $E_a$, shown in Figure 4B, clearly demonstrates the compensation effect in our catalytic system. Although the compensation effect is very common in heterogeneous catalysis and a large number of homogeneous systems,[27−30] the mechanism is still not completely understood. According to the switching theory

**TABLE 1. Summary of the Reaction Rate Constant ($k$) and Adsorption Time ($t_{ads}$) at Three Different Temperatures for the Au-Based Nanocages, Nanoboxes, Partially Hollow Nanoboxes, and Solid Nanoparticles**

| | 9 °C | | 24 °C | | 43 °C | |
|---|---|---|---|---|---|---|
| | $k$ (min$^{-1}$) | $t_{ads}$ (min) | $k$ (min$^{-1}$) | $t_{ads}$ (min) | $k$ (min$^{-1}$) | $t_{ads}$ (min) |
| nonocages | 1.54 ± 0.10 | 1.84 ± 0.20 | 2.83 ± 0.11 | 0.64 ± 0.08 | 5.58 ± 0.17 | 0.18 ± 0.04 |
| nanoboxes | 0.43 ± 0.03 | 6.41 ± 0.52 | 1.12 ± 0.02 | 1.56 ± 0.29 | 3.25 ± 0.28 | 0.23 ± 0.02 |
| partially hollow nanoboxes | 0.17 ± 0.02 | 8.66 ± 0.73 | 0.59 ± 0.04 | 2.09 ± 0.32 | 2.16 ± 0.18 | 0.27 ± 0.08 |
| solid nonparticles (50 nm) | | | 0.20 ± 0.02 | 0.40 ± 0.04 | | |
| solid nonparticles (5 nm) | | | 0.95 ± 0.08 | 0.05 ± 0.01 | | |



DOI: 10.1021/nl903062e | *Nano Lett.* **2010,** *10,* 30-35

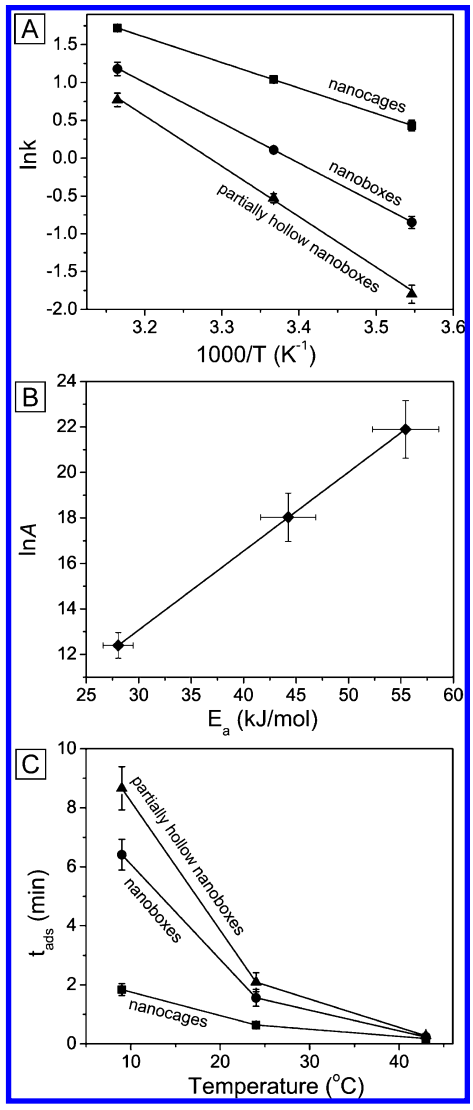


**FIGURE 4. (A) The Arrhenius plots for reactions catalyzed by nanocages, nanoboxes, and partially hollow nanoboxes. The activation energy ($E_a$) can be calculated from the slope of the linear fitting in each case. (B) Plot of pre-exponential factors (ln $A$) versus $E_a$ of the Arrhenius equation, demonstrating the compensation effect for catalysts based on Au nanocages or nanoboxes. (C) Temperature-dependent absorption time ($t_{ads}$) for nanocages, nanoboxes, and partially hollow nanoboxes, respectively.**

proposed by Bligaard and co-workers,[28] we believe this effect should be related to a switching in kinetics, from a regime where the overall rate is dominated by the rate of activation of the reactant (i.e., *p*-nitrophenolate) to a regime where the stability of the reaction product (i.e., *p*-aminophenol) adsorbed on the surface of the catalyst becomes more important. In the case of partially hollow nanoboxes, the apparent $E_a$ was relatively high, while the adsorption of the reduction product on the surface of nanoboxes was less stable because of the relatively low density of active site (if one only takes into account the Au atoms on the surface). On the other hand, for the reaction with Au nanocages, $E_a$ was lower while the relatively high density of reactive site would contribute greatly to the stability of such adsorption. Therefore, the compensation effect could be qualitatively interpreted using the switching theory.

Another interesting observation is the variation in adsorption period (i.e., $t_{ads}$ shown in parts B–D of Figure 2, Figure 3, and Table 1). We assume that the rate of adsorption of *p*-nitrophenol on the surface of a catalyst is the predominant factor in the induction period. The adsorption of *p*-nitrophenol might play an important role in activating the reaction. Accordingly, it is not difficult to understand why the larger specific surface area the catalyst possesses, the faster the reactant will be activated, and the shorter the induction period will be.

It is also worth mentioning that there are two interesting phenomena at the beginning of the reduction when we used spherical Au solid nanoparticles of different sizes (5 and 50 nm) as the catalyst for comparison (see Figure 2B, Figure 3B, and Table 1). First, the $t_{ads}$ for both the Au solid nanoparticles were shorter than any of the other three porous systems and relied on the particle size, probably due to their solid morphology and thus the well-known size effect. Second, according to our analysis and interpretation above, the solid nanoparticles should exhibit a lower reaction rate than the other three catalysts because of its much lower surface-to-volume ratio. However, the reaction rates in the beginning period were faster than what we anticipated. Given that the Au solid nanoparticles were capped by citrate group instead of poly(vinylpyrrolidone) (PVP), we believe that the citrate group might be able to act as a reductant in the system. In order to confirm our assumption, we conducted a control experiment by only adding trisodium citrate instead of citrate-capped nanoparticles into the reacting system. The results shown in Figure S2 (in Supporting Information) clearly demonstrate the capability for citrate group to directly reduce *p*-nitrophenol quickly. Hence, after taking into account the interference of citrate ions, the calculated average reaction rate constants for Au solid nanoparticles were $0.20 \pm 0.02$ min$^{-1}$ (for 50 nm particles) and $0.95 \pm 0.08$ min$^{-1}$ (for 5 nm particles); both of them were much smaller than that of nanocages at 24 °C. Consequently, the catalytic activity of porous Au nanocages was significantly higher than those of Au solid nanoparticles,

**TABLE 2. Summary of the Activation Energy ($E_a$), Pre-Exponential Factors ($A$), and the Entropy of Activation ($\Delta S$) for the Nanocages, Nanoboxes, and Partially Hollow Nanoboxes**

| | $E_a$ (kJ/mol) | $A$ (min$^{-1}$) | $\Delta S$ (J/mol·K) |
|---|---|---|---|
| nonocages | 28.04 ± 1.43 | 1.3–4.2 (×10$^5$) | 103.05 ± 4.68 |
| nanoboxes | 44.25 ± 2.62 | 2.3–19.5 (×10$^7$) | 149.90 ± 8.83 |
| partially hollow nanoboxes | 55.44 ± 3.15 | 0.9–11.5 (×10$^9$) | 182.05 ± 10.05 |



DOI: 10.1021/nl903062e | *Nano Lett.* **2010,** *10,* 30-35

even when the size of the Au nanoparticles is on the same scale as the wall thickness of the Au nanocages. The considerable enhancement in catalytic activity for the Au nanocages can be probably attributed to the following two factors: (i) the nanocage could provide a much larger surface (per particle) than a small solid nanoparticle to simultaneously accommodate both the oxidation and reduction half reactions and (ii) the ultrathin walls of the nanocage could provide a much higher activity than a big solid nanoparticle due to the size effect. In other words, the superior catalytic activity of the Au nanocages is a result of two effects—good electrical connection and small size—related to their ultrathin and highly porous walls. We also benchmarked the catalytic activity of the Au nanocages against some systems that have been reported in the literature. The $k$ value for the Au nanocages at room temperature is at least 1 order of magnitude higher than those reported for Au nanoparticles with sizes ranging from 5 to 50 nm.[24,25,32,33] In fact, the $k$ value for the Au nanocages is very close to the value reported for Pt nanoparticles supported on polymers.[34] These results indicate that the catalytic performance of Au nanostructures could be greatly enhanced by controlling both the morphology and porosity through refinement of the synthesis.

In summary, we have demonstrated the use of Au-based nanocages and nanoboxes as new catalysts for the reduction of *p*-nitrophenol by $NaBH_4$. We have also obtained the relationship between the catalytic activity and the particle morphology: that is, the more open the particle morphology is and the thinner the wall is, and the higher the catalytic activity will be. The good intrinsic electrical connection across the entire surface of a Au nanocage makes it a much better catalyst than small Au solid nanoparticles for a redox reaction. In addition, a typical compensation effect was observed in this catalytic system, which can be explained by the assumption of kinetic regime switching. Given the high abundance of Au element relative to other noble metals like Pt and Pd as well as the easiness in controlling the porosity and morphology, the Au-based nanocages might be able to find widespread use as catalysts in a number of industrial applications.

**Acknowledgment.** This work was supported in part by a research grant from the NSF (DMR-0804088) and startup funds from Washington University in St. Louis. Y.X. thanks the WCU program of MEST in Korea for a partial support. As a visiting Ph.D. student from University of Science and Technology of China, Q.Z. was also partially supported by the China Scholarship Council. Part of the work was performed at the Nano Research Facility (NRF), a member of the National Nanotechnology Infrastructure Network (NNIN), which is supported by the NSF under award no. ECS-0335765. NRF is part of the School of Engineering and Applied Science at Washington University in St. Louis.

**Supporting Information Available.** Description of experimental procedures and figures showing TEM image of Au nanoparticles and extinction spectra before and after addition of trisodium citrate. This material is available free of charge via the Internet at http://pubs.acs.org.

## REFERENCES AND NOTES

(1) Elghanian, R.; Storhoff, J. J.; Mucic, R. C.; Letsinger, R. L.; Mirkin, C. A. *Science* **1997**, *277*, 1078.
(2) Bruchez, M.; Moronne, M.; Gin, P.; Weiss, S.; Alivisatos, A. P. *Science* **1998**, *281*, 2013.
(3) Empedocles, S. A.; Bawendi, M. G. *Science* **1997**, *278*, 2114.
(4) Ghosh, S. K.; Pal, T. *Chem. Rev.* **2007**, *107*, 4797.
(5) Lee, J. S.; Ulmann, P. A.; Han, M. S.; Mirkin, C. A. *Nano Lett.* **2008**, *8*, 529.
(6) Hirsch, L. R.; Stafford, R. J.; Bankson, J. A.; Sershen, S. R.; Rivera, B.; Price, R. E.; Hazle, J. D.; Halas, N. J.; West, J. L *Proc. Natl. Acad. Sci. U.S.A.* **2003**, *100*, 13549.
(7) Murphy, C. J.; Gole, A. M.; Hunyadi, S. E.; Orendorff, C. J. *Inorg. Chem.* **2006**, *45*, 7544.
(8) Zeng, J.; Huang, J.; Lu, W.; Wang, X.; Wang, B.; Zhang, S.; Hou, J. *Adv. Mater.* **2007**, *19*, 2172.
(9) Chen, J. Y.; McLellan, J. M.; Siekkinen, A.; Xiong, Y. J.; Li, Z. Y.; Xia, Y. N. *J. Am. Chem. Soc.* **2006**, *128*, 14776.
(10) Skrabalak, S. E.; Au, L.; Li, X. D.; Xia, Y. *Nat. Protoc.* **2007**, *2*, 2182.
(11) Skrabalak, S. E.; Chen, J. Y.; Sun, Y. G.; Lu, X. M.; Au, L.; Cobley, C. M.; Xia, Y. N. *Acc. Chem. Res.* **2008**, *41*, 1587.
(12) Chen, J.; Saeki, F.; Wiley, B. J.; Cang, H.; Cobb, M. J.; Li, Z. Y.; Au, L.; Zhang, H.; Kimmey, M. B.; Li, X. D.; Xia, Y. *Nano Lett.* **2005**, *5*, 473.
(13) Chen, J. Y.; Wang, D. L.; Xi, J. F.; Au, L.; Siekkinen, A.; Warsen, A.; Li, Z. Y.; Zhang, H.; Xia, Y. N.; Li, X. D. *Nano Lett.* **2007**, *7*, 1318.
(14) Chen, J. Y.; Wiley, B.; Li, Z. Y.; Campbell, D.; Saeki, F.; Cang, H.; Au, L.; Lee, J.; Li, X. D.; Xia, Y. N. *Adv. Mater.* **2005**, *17*, 2255.
(15) Skrabalak, S. E.; Chen, J.; Au, L.; Lu, X.; Li, X.; Xia, Y. *Adv. Mater.* **2007**, *19*, 3177.
(16) Yang, X. M.; Skrabalak, S. E.; Li, Z. Y.; Xia, Y. N.; Wang, L. H. V. *Nano Lett.* **2007**, *7*, 3798.
(17) Au, L.; Zheng, D. S.; Zhou, F.; Li, Z. Y.; Li, X. D.; Xia, Y. N. *ACS Nano* **2008**, *2*, 1645.
(18) Song, K. H.; Kim, C. H.; Cobley, C. M.; Xia, Y. N.; Wang, L. V. *Nano Lett.* **2009**, *9*, 183.
(19) Daniel, M. C.; Astruc, D. *Chem. Rev.* **2004**, *104*, 293.
(20) Min, B. K.; Friend, C. M. *Chem. Rev.* **2007**, *107*, 2709.
(21) Sun, Y. G.; Xia, Y. N. *J. Am. Chem. Soc.* **2004**, *126*, 3892.
(22) Schrinner, M.; Ballauff, M.; Talmon, Y.; Kauffmann, Y.; Thun, J.; Moller, M.; Breu, J. *Science* **2009**, *323*, 617.
(23) Lee, J.; Park, J. C.; Song, H. *Adv. Mater.* **2008**, *20*, 1523.
(24) Hayakawa, K.; Yoshimura, T.; Esumi, K. *Langmuir* **2003**, *19*, 5517.
(25) Praharaj, S.; Nath, S.; Ghosh, S. K.; Kundu, S.; Pal, T. *Langmuir* **2004**, *20*, 9889.
(26) Narayanan, R.; El-Sayed, M. A. *Nano Lett.* **2004**, *4*, 1343.
(27) Zsako, J. *J. Therm. Anal.* **1996**, *47*, 1679.
(28) Bligaard, T.; Honkala, K.; Logadottir, A.; Norskov, J. K.; Dahl, S.; Jacobsen, C. J. H. *J. Phys. Chem. B* **2003**, *107*, 9325.
(29) Patterson, W. R.; Rooney, J. J. *J. Catal.* **1994**, *146*, 310.
(30) Rooney, J. J. *J. Mol. Catal. A: Chem.* **1998**, *129*, 131.
(31) Rashid, M. H.; Mandal, T. K. *Adv. Funct. Mater.* **2008**, *18*, 2261.
(32) Dotzauer, D. M.; Dai, J.; Sun, L.; Bruening, M. L. *Nano Lett.* **2006**, *6*, 2268.
(33) Rashid, M. H.; Bhattacharjee, R. R.; Kotal, A.; Mandal, T. K. *Langmuir* **2006**, *22*, 7141.
(34) Esumi, K.; Isono, R.; Yoshimura, T. *Langmuir* **2004**, *20*, 237.



DOI: 10.1021/nl903062e | *Nano Lett.* **2010,** *10,* 30-35